Competing interests statement

The authors declare that they have no competing financial interests.

Correspondence and requests for materials should be addressed to R.R. (e-mail: rreed@hms.harvard.edu), K.S. (e-mail: Kevin@hms.harvard.edu) or E.H. (e-mail: cg5@ix.urz.uni-heidelberg.de).

The dynamics of actin-based motility depend on surface parameters

Anne Bernheim-Groswasser*, Sebastian Wiesner†, Roy M. Golsteyn*‡, Marie-France Carlier† & Cécile Sykes*

** Laboratoire Physico-chimie 'Curie', UMR 168 CNRS/Institut Curie, 11, rue Pierre et Marie Curie, 75231 Paris cedex 05, France*
† Dynamique du Cytosquelette, Laboratoire d'Enzymologie et Biochimie Structurales, UPR A 9063 CNRS, 91198 Gif-sur-Yvette, France

In cells, actin polymerization at the plasma membrane is induced by the recruitment of proteins such as the Arp2/3 complex, and the zyxin/VASP complex[1–3]. The physical mechanism of force generation by actin polymerization has been described theoretically using various approaches[4–6], but lacks support from experimental data. By the use of reconstituted motility medium[7], we find that the Wiskott–Aldrich syndrome protein[8,9] (WASP) subdomain, known as VCA, is sufficient to induce actin polymerization and movement when grafted on microspheres. Changes in the surface density of VCA protein or in the microsphere diameter markedly affect the velocity regime, shifting from a continuous to a jerky movement resembling that of the mutated 'hopping' *Listeria*[10]. These results highlight how simple physical parameters such as surface geometry and protein density directly affect spatially controlled actin polymerization, and play a fundamental role in actin-dependent movement.

Investigations of the pathogens *Listeria monocytogenes* and *Shigella flexneri* were important in identifying many proteins that control cellular actin polymerization and cell motility. These bacteria move within a cell by inducing actin polymerization at their surface[11] by way of the activation of the Arp2/3 complex[12,13]. Immunolocalization studies of the Arp2/3 complex in the lamellipodium[14] show that Arp2/3 multiplies the filaments by branching them in a dendritic array[15], as confirmed by biochemical experiments[16,17]. More recently, surfaces coated with proteins that induce actin polymerization were used to identify new molecular partners for actin polymerization and assembly[18], or to visualize microscopically the actin network formed at the surface[19].

Here we consider how the surface concentration of Arp2/3 complex activator, or the curvature of the surface on which filament branching and growth occur, can affect and control actin-based movement. We have used beads of various diameters (1–10 μm) grafted with the VCA fragment (VCA indicates verprolin-homology, cofilin-homology, and acidic regions), which constitutively activates Arp2/3 complex. We placed the beads in a medium containing a minimal number of purified proteins that support the movement of *L. monocytogenes* or *S. flexneri*[7]. After a certain time that depends on their size, the beads generated behind them a comet (tail) made of actin filaments and started moving. We identified three main characteristic regimes of motion: continuous (smooth), intermittent or erratic, and periodic or saltatory movement. We believe that this is the first evidence that transition from continuous to saltatory movement can be achieved simply by a change in a physical parameter—that is, the surface density or the bead diameter.

The VCA-coated beads[18] (1–10 μm in diameter) all had the same saturating surface density C_s of VCA, as confirmed by SDS–polyacrylamide gel electrophoresis (SDS–PAGE) (data not shown). We placed the beads in the mixture of purified proteins[7], and found that the bead size had a significant effect on the movement type and the comet structure (Fig. 1). Small beads (1–2 μm diameter) moved steadily at a constant velocity (Fig. 1a), as reported in other experimental systems[20]. Unexpectedly, larger beads displayed a jerky motion. The irregularities in the movement are illustrated by the irregular density (grey level) of the comet (Fig. 1b and c). Furthermore, beads larger than 4.5 μm diameter moved in a periodic hopping manner (Fig. 1c), very similar to the movement of mutated 'hopping' *Listeria*[10]. For intermediate-sized beads (3 μm in diameter), a transient or even chaotic movement was observed: the beads hopped randomly, fluctuating from smooth to jerky movement (Fig. 1b). All beads of the same nominal diameter developed comets and showed the same type of motion when sampling the microscope field of view (typically up to 50 beads), showing the robustness of the system.

In these experiments, the surface density of VCA proteins on beads of different diameter was $C_s = (6 \pm 1) \times 10^{-2}$ molecules nm^{-2}. This value corresponds to a maximal surface concentration of VCA. The capacity of immobilized VCA to activate Arp2/3 was evaluated and compared with the activity of VCA in the soluble form using the fluorescence of pyrenyl-actin to monitor the polymerization process. The assay was carried out with identical amounts of immobilized or soluble VCA in parallel. This proved that the specific activity of VCA was the same in both cases, and that the surface concentration of active VCA was independent of the size of the bead.

Mean velocity values, V_{mean}, of beads moving in the solution of purified proteins are given in Table 1. This mean velocity is linearly dependent on the inverse bead diameter. Beads of 1 μm diameter placed in the mixture of purified proteins or in HeLa cell extracts (prepared as previously described[21]) moved with the same average velocity. But in purified protein solution, 100% of the beads started moving by breaking the surrounding symmetrical actin gel ('symmetry breaking') within a few minutes, whereas in the case of cell extracts, symmetry breaking occurred only after 20 minutes and for less than 10% of the beads. Moreover, the velocity fluctuations in the movement of a single bead were 70% in purified proteins as compared to 15% in cell extracts. This can be related to the lower viscosity of the purified protein mixture, as shown in a recent

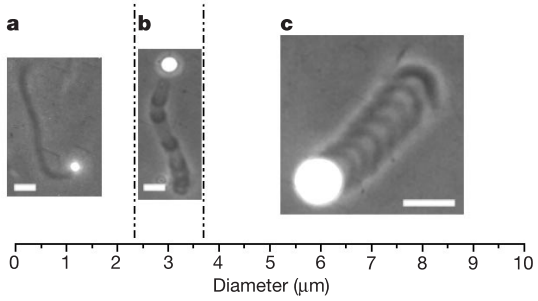

Figure 1 The three main regimes of motion of the beads as a function of bead diameter. In all cases, the beads have a saturated surface concentration of VCA. The dashed vertical lines mark the approximate boundaries between these regimes. **a**, Small beads (<2.5 μm diameter) with a comet of constant gel density (grey level) exhibit continuous motion. **b**, Medium-size beads of 3 μm diameter move in an intermittent manner, as manifested by the irregular gel density of the comet. **c**, Large beads (≥4.5 μm diameter) progress in periodic fashion, as reflected by the alternating comet grey level. Scale bars: **a** and **b**, 5 μm; **c**, 10 μm.

‡ Present address: Division de Cancérologie Expérimentale, Institut de Recherches Servier, 125, chemin de Ronde, 78290 Croissy-sur-Seine, France.

quantitative analysis of *Listeria* movement in fibroblasts[22]. Beads of diameter >3 μm placed in cell extracts only rarely produced a comet, and could not be statistically characterized.

Using video phase-contrast optical microscopy, we measured two quantities as a function of time t: the curvilinear distance $D(t)$ from the end of the comet to the bead centre, and the velocity (the time derivative $dD(t)/dt$). These two quantities are respectively plotted in Fig. 2a and b for a 4.5-μm bead at C_s moving in a periodic fashion. Even though actin depolymerization occurs, the end of the comet remained visible until the end of the experiment. The beads that move periodically display a periodic comet structure (Fig. 1c). Analysis of the grey-level intensity of the actin gel along the comet as a function of the distance $X = D(t) - R$, where R is the bead radius, was carried out on a final image. The time dependence of the grey intensity was deduced (Fig. 2c). A correlation was observed between velocity and grey-scale intensity along the comet (Fig. 2b and c, respectively). The velocity of the bead is maximal when the gel density is minimal (low grey level) and vice versa. This correlation can be explained by means of an elastic analysis[5,23] (see Supplementary Information). In this analysis, a friction force F_f, opposing a propulsion force F_e, results from the connection of the gel (via VCA molecules) to the surface of the bead. The model shows that if the molecular connections can break, the friction will depend non-monotonically on the velocity[5,23]. Consequently, saltatory and continuous regimes are predicted.

The characteristic distance ΔD_{cycle} determined by fast Fourier transform (FFT) analysis of the grey-scale intensity as a function of X is 5.0 ± 0.8 μm, which corresponds to the average size of a step (Fig. 2a). The characteristic time ΔT_{cycle} (also determined by FFT analysis) is 10.7 ± 2.0 minutes. This time is independent of the bead diameter within experimental error, in contrast to ΔD_{cycle} that decreases with the bead size: for 6 μm, $\Delta D_{cycle} = 3.8 \pm 0.3$ μm, whereas for 10 μm, $\Delta D_{cycle} = 2.5 \pm 0.4$ μm. For 6-μm-diameter beads and above, the uncertainty in ΔD_{cycle} is rather small (about 10%) and reflects a better-defined period than for 4.5-μm-diameter beads. Stepping behaviour at a molecular scale (5.4 nm) was reported for *Listeria*[24], and these authors suggest that it may reflect a highly coordinated progress along many filaments, or discrete events of individual actin filament attachment/detachment to the bacterial surface, which is more likely. We believe that the macroscopic steps on the micrometre length scale observed in our experiments represent a phenomenon that results from a coordinated collective process of a large number of connected (branched) filaments. The two phenomena may act in concert, but our experimental set-up cannot detect discrete molecular events.

Table 1 Diameter and mean velocity of beads

Diameter (μm)	V_{mean} (μm min^{-1})
0.954 ± 0.028	1.1 ± 0.2
2.134 ± 0.039	0.63 ± 0.13
2.837 ± 0.133	0.54 ± 0.11
4.537 ± 0.236	0.49 ± 0.12
6.348 ± 0.455	0.34 ± 0.07
9.14 ± 0.709	0.29 ± 0.04

Mean velocity values, V_{mean}, as a function of bead diameter. The values are measured on about 10 beads as the ratio of the curvilinear accumulated distance over time. For beads with diameter >3 μm, the velocity has been averaged over 1.5 h. A linear dependence was found between the mean velocity and the inverse diameter of the beads.

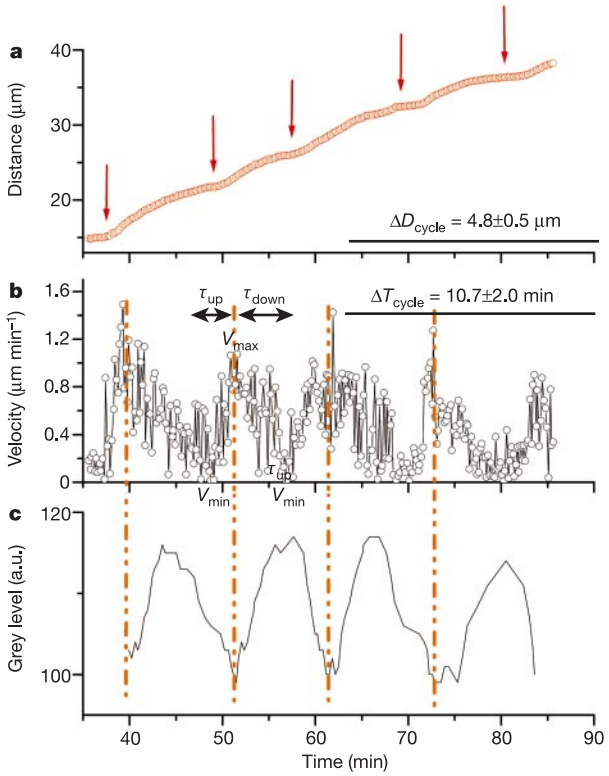

Figure 2 The characteristic behaviour of a 4.5-μm bead at a saturated VCA surface density C_s. The bead exhibits a periodic movement as shown. **a**, The travelled distance (from the comet end to the bead centre) as a function of time shows stepping behaviour. The arrows mark the time of minimum velocity (V_{min}). **b**, The velocity as a function of time, obtained from the time derivative of the travelled distance (**a**), is periodic. During one cycle, the bead accelerates from V_{min} to V_{max} in a time τ_{up} and decelerates to V_{min} with a longer time τ_{down}. The distance accumulated during a step (a jump), ΔD_{cycle}, is 5.0 ± 0.8 μm, averaged over ten beads, the error representing the standard deviation. The characteristic cycle time ΔT_{cycle} is 10.7 ± 2.0 min, where the error is determined by the full-width at half-maximum of the FFT curve. This time was found to be independent of the bead diameter. **c**, The grey level of the generated actin gel behind the bead as a function of time is shown. The dashed lines show the correlation between minimum grey level (low gel density) and maximum bead velocity.

We studied the dependence of the comet curvature K on the bead diameter D at constant surface density C_s of VCA (see Supplementary Information). We found a power-law dependence, with K proportional to $D^{-(1.1 \pm 0.1)}$. If we consider that the density of actively pushing filaments is constant for all beads, an analysis[25] of the bead trajectories based on the Elastic Brownian Ratchet (EBR) model predicts a power of -2, which is not in agreement with our results. A possible reason for this discrepancy is the assumption[25] that each pushing filament is randomly placed on the surface, whereas in practice the filaments are connected and their actions can be correlated.

An early step in actin-based motility of spherical objects in cells, such as lysosomes and endocytic vesicles[26,27], is the breakage of the symmetrical actin gel that surrounds the bead[28]. We characterized symmetry breaking by measuring the time from the instant the beads were placed into the motility medium until they started to move. This time increased linearly with the diameter of the beads (Fig. 3). This linearity can be understood by considering that the actin gel is under tension. Owing to spherical geometry, the growing actin gel is stretched, which results in the development of a lateral stress, $\sigma_{\theta\theta}$, that is maximal at the outer surface of the gel. In turn, the stretched gel exerts a normal stress on the bead[21]. $\sigma_{\theta\theta}$ depends on the Young's modulus C, the thickness of the gel, e, and the radius of the bead, R, as $\sigma_{\theta\theta} = Ce/R$. This relation is still valid at the time the gel fractures. If the thickness of the gel at that time is sufficiently smaller than its thickness in the stationary condition, then e increases linearly with time as a function of the polymerization velocity v_p: $e = v_p t$.

The time of symmetry breaking is given by:

$$t_c = \frac{\sigma^c_{\theta\theta}}{v_p}\frac{R}{C} = \alpha R = \frac{\alpha}{2}D$$

where $\sigma^c_{\theta\theta}$ is the critical stress necessary to initiate a fracture; t_c is proportional to the radius, or the bead diameter D. We can estimate the validity of this model by evaluating the slope $a = \alpha/2$. We observed experimentally that the ratio e/R is of the order of 1, and using the relation $\sigma^c_{\theta\theta} = Ce/R$ we deduce that $\alpha = 1/v_p$. The experimental value of the slope a is $2.1 \pm 0.2\ \mathrm{min\,\mu m^{-1}}$, thus $\alpha = 4.2 \pm 0.4\ \mathrm{min\,\mu m^{-1}}$ and we find that $v_p = 0.24 \pm 0.02\ \mathrm{\mu m\,min^{-1}}$. This value is about one order of magnitude smaller than the value we obtained in stress-free pyrene assay measurements, owing to the stress exerted on the surface[21]. The value of t_c changes with the VCA surface density—for example, for 6-μm beads, t_c increases when the VCA concentration decreases. In cells, vesicle size and membrane composition are probably determining factors for symmetry breaking.

To find out how the surface density of VCA controls motility, we tested beads (4.5 μm in diameter) coated with different concentrations of VCA. Decreasing the VCA surface concentration by a factor of 2 (50% saturation of the surface, as determined by SDS–PAGE analysis) induces a transition from saltatory to continuous motion (data not shown). This transition can be related to the drop in the friction force due to the reduction of the surface density of VCA, as qualitatively explained by the elastic analysis[5,23]. The surface concentration of active VCA was measured using polymerization assay, and was found to be one-sixth of the value under saturating conditions. At concentrations corresponding to a 50-fold decrease of active VCA, no movement was detected. The surface concentration at which the transition occurs was found to depend on the bead diameter.

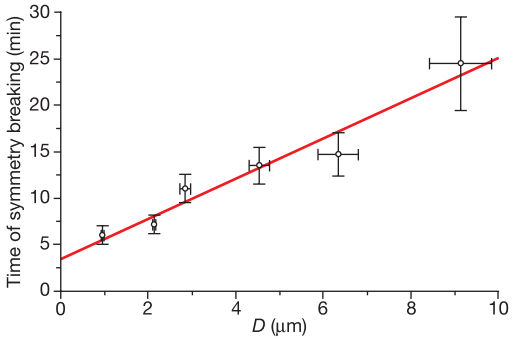

Figure 3 The linear dependence between the time of symmetry breaking and the bead diameter. The slope is $a = \alpha/2 = 2.1 \pm 0.2\ \mathrm{min\,\mu m^{-1}}$. The error in the bead diameter is given by the manufacturer, and the error in the time of symmetry breaking is calculated statistically using 10 beads.

Although the system described here is far from the complexity of a cell, the use of a limited set of proteins enabled us to identify the physical relationship between surface geometry and the Arp2/3 complex-dependent actin polymerization. It also shows that relevant concentrations of proteins may have important implications for actin-dependent morphogenesis in cell protrusions, as recently shown in cultured cells[29]. If actin polymerization is capable of deforming a plasma membrane, or, in other words, changing the surface geometry, then the resulting changes in membrane shape can affect subsequent polymerization at the same site—and consequently further out, owing to elasticity. More-complex biochemical changes, such as activation of small GTPases or protein phosphorylation, may act on these inherent physical parameters rather than directly induce the cell movement. Furthermore, we note that changes in physical parameters can mimic the phenotype of the 'hopping' *Listeria*, which was previously induced by altering the ActA protein sequence[10]. The ability of physical parameters to reproduce a protein effect greatly enlarges the scope of cellular actin cytoskeleton dynamics, and hence offers more ways to explain the wide range of actin structures within cells at a local level. □

Methods

Derivatization of beads with VCA

VCA was bacterially expressed as a glutathione *S*-transferase (GST) fusion protein by inserting the corresponding DNA fragments from pSRα-Puro in a modified version of pGEX-4T-1 with an extra *Spe*I site. The stock solution was 1.5 mg ml^{-1}, as determined by Bradford assay.

Polystyrene beads of diameter ranging from 1 to 10 μm were purchased from Polyscience. Beads were incubated in the VCA solution at concentrations in the range of 0.01–1 mg ml^{-1} for one hour at room temperature. We used an initial volume of beads that was proportional to the diameter: that is, volumes of 1 μl and 10 μl for beads of 1 μm and 10 μm diameter respectively, given that the volume fraction of the beads in the stock solution was constant, equal to 2.5%. The beads were finally re-suspended in a constant total volume of 20 μl to ensure a constant total surface area of the beads independent of the bead diameter. The beads were stored at 4 °C in a storage buffer (20 mM phosphate buffer, pH 7.4, 150 mM NaCl, 1.5 mM NaN_3, 10 mg ml bovine serum albumin (BSA), 5% glycerol) for up to 1 week. We varied the protein concentration on the surface by changing the protein concentration in the incubating solution.

Motility assay

The motility medium contained 8.5 mM HEPES, pH 7.7, 1.7 mM Mg-ATP, 5.5 mM dithiothreitol, 0.12 mM Dabco, 0.1 M KCl, 1 mM $MgCl_2$, 6.5 μM F-actin, 0.1 μM Arp2/3 complex, 0.046 μM capping proteins, 2.5 μM actin depolymerizing factor (ADF), 2.5 μM profilin, 0.54 μM α-actinin, 0.31% methyl-cellulose, 0.75% BSA, 1.1 μM actin-rhodamin as optimized for *Listeria* movement[7]. No vasodilator-simulated phosphoprotein (VASP) was needed. A 0.3-μl volume of bead suspension was added to 20 μl of motility medium. The small volume of the beads ensured that the composition of the motility medium remained unchanged. The sample was placed immediately between a glass slide and a glass coverslip 18 × 18 mm, sealed with vaseline:lanolin:paraffin (at weight ratio of 1:1:1). To prevent squeezing of the objects, the distance between slide and coverslip was controlled using an inert polyethylene glycol spacer (Goodfellow) to obtain a ratio between sample height and bead diameter of 5 to 6. We found that this ratio ensured that the beads with their comets do not stick to the coverslip walls. In all experiments, symmetry breaking occurs spontaneously, and 100% of the beads generate a comet.

The movement of the microspheres was followed for 1.5 hours by time-lapse optical video-microscopy (phase contrast and fluorescence microscopy, Olympus microscope, ×100). Measurements of bead velocity and the grey-level intensity along the comets were performed using METAMORPH and a software program consisting of a user module (O. Cardoso) for NIH Image (W. Rasband, National Institutes of Health). Both source code and compiled application for MacOS are available at http://canardo.lbhp.jussieu.fr/cardoso/. In order to obtain a statistical weight for the data, at the end of the experiment

we measured the grey-scale intensity of the comets developed by the tracked beads as well as by other ones (about 10).

Determination of activity of immobilized VCA using a polymerization assay

VCA activity was measured as the maximal rate of polymerization of pyrenyl-actin (2.5 μM) in the presence of Arp2/3 complex (20 nM) and VCA at different concentrations as described[13]. A calibration curve was first established using known concentrations of soluble VCA. The polymerization assays were then performed by adding immobilized VCA in the fluorescence cuvette. 16% sucrose (w/v) was included in the polymerization buffer to prevent sedimentation of the polystyrene beads. The concentration of active immobilized VCA was determined by comparison of the rates measured using VCA-derivatized beads with the calibration curve as a function of soluble VCA. The concentration of actually immobilized VCA was derived from SDS–PAGE. The specific activity of immobilized VCA was derived.

Received 9 January; accepted 20 March 2002.

1. Welch, M. D., Mallavarapu, A., Rosenblatt, J. & Mitchison, T. J. Actin dynamics in vivo. *Curr. Opin. Cell. Biol.* **9,** 54–61 (1997).
2. Renfranz, P. J. & Beckerle, M. C. Doing (F/L)PPPPS: EVH1 domains and their proline-rich partners in cell polarity and migration. *Curr. Opin. Cell Biol.* **14,** 88–103 (2002).
3. Pantaloni, D., Le Clainche, C. & Carlier, M.-F. Mechanism of actin-based motility. *Science* **292,** 1502–1506 (2001).
4. Mogilner, A. & Oster, G. Cell motility driven by actin polymerisation. *Biophys. J.* **71,** 3030–3045 (1996).
5. Gerbal, F., Chaikin, P., Rabin, Y. & Prost, J. An elastic analysis of *Listeria monocytogenes* propulsion. *Biophys. J.* **79,** 2259–2275 (2000).
6. Carlsson, A. E. Growth of branched actin networks against obstacles. *Biophys. J.* **81,** 1907–1923 (2001).
7. Loisel, T. P., Boujemaa, R., Pantaloni, D. & Carlier, M.-F. Reconstitution of actin-based motility of *Listeria* and *Shigella* using pure proteins. *Nature* **401,** 613–616 (1999).
8. Machesky, L. M. & Insall, R. H. Scar1 and the related Wiskott–Aldrich syndrome protein, WASP regulates the actin cytoskeleton through the Arp2/3 complex. *Curr. Biol.* **8,** 1347–1356 (1998).
9. Takenawa, T. & Miki, H. WASp and WAVE family proteins: key molecules for rapid rearrangement of cortical actin filaments and cell movement. *J. Cell Sci.* **114,** 1801–1809 (2001).
10. Lasa, I. *et al.* Identification of two regions in the N-terminal domain of ActA involved in the actin comet tail formation by *Listeria monocytogenes*. *EMBO J.* **16,** 1531–1540 (1997).
11. Tilney, L. G. & Portnoy, D. A. Actin filaments and the growth, movement, and spread of the intracellular bacterial parasite, *Listeria monocytogenes*. *J. Cell Biol.* **109,** 1597–1608 (1989).
12. Welch, M. D., Iwamatsu, A. & Mitchison, T. J. Actin polymerisation is induced by Arp2/3 protein complex at the surface of *Listeria monocytogenes*. *Nature* **385,** 265–268 (1997).
13. Egile, C. *et al.* Activation of Cdc42 effector N-WASP by the Shigella IcsA protein promotes actin nucleation by Arp2/3 complex resulting in bacterial actin-based motility. *J. Cell. Biol.* **146,** 1319–1332 (1999).
14. Svitkina, T. M. & Borisy, G. G. Arp2/3 complex and actin polymerizing factor/cofilin in dendritic organization and treadmilling of actin filament array in lamellipodia. *J. Cell Biol.* **145,** 1009–1026 (1999).
15. Mullins, R. D., Heuser, J. A. & Pollard, T. D. The interaction of Arp2/3 complex with actin: nucleation, high affinity pointed end capping, and formation of branching networks of filaments. *Proc. Natl Acad. Sci. USA* **95,** 6181–6186 (1998).
16. Blanchoin, L. *et al.* Direct observation of dendritic actin filaments networks nucleated by Arp2/3 complex and WASP/Scar proteins. *Nature* **404,** 1007–1011 (2000).
17. Pantaloni, D., Boujemaa, R., Didry, D., Gounon, P. & Carlier, M.-F. The Arp2/3 complex branches filament barbed ends: functional antagonism with capping proteins. *Nature Cell Biol.* **2,** 385–391 (2000).
18. Fradelizi, J. *et al.* ActA and human zyxin harbour Arp2/3-independent actin-polymerisation activity. *Nature Cell Biol.* **3,** 699–707 (2001).
19. Cameron, L. A., Svitkina, T. M., Vignjevic, D., Theriot, J. A. & Borisy, G. G. Dendritic organization of actin comet tails. *Curr. Biol.* **11,** 130–135 (2001).
20. Cameron, L. A., Footer, M. J., van Oudenaarden, A. & Theriot, J. A. Motility of ActA protein-coated microspheres driven by actin polymerisation. *Proc. Natl Acad. Sci. USA* **96,** 4908–4913 (1999).
21. Noireaux, V. *et al.* Growing an actin gel on spherical surfaces. *Biophys. J.* **78,** 1643–1654 (2000).
22. Giardini, P. A. & Theriot, J. A. Effects of intermediate filaments on actin-based motility of *Listeria monocytogenes*. *Biophys. J.* **81,** 3193–3203 (2001).
23. Gerbal, F. *et al.* On the '*Listeria*' propulsion mechanism. *Pramana J. Phys.* **53,** 155–170 (1999).
24. Kuo, S. C. & McGrath, L. Steps and fluctuations of *Listeria monocytogenes* during actin-based motility. *Nature* **407,** 1026–1029 (2000).
25. Rutenberg, A. D. & Grant, M. Curved tails in polymerization-based bacterial motility. *Phys. Rev. E* **64,** 21904–21907 (2001).
26. Merrifield, C. J. *et al.* Endocytic vesicles move at the tips of actin tails in cultured mast cells. *Nature Cell Biol.* **1,** 72–74 (1999).
27. Taunton, J. *et al.* Actin-dependent propulsion of endosomes and lysosomes by recruitment of N-WASP. *J. Cell Biol.* **148,** 519–530 (2000).
28. Van Oudenaarden, A. & Theriot, J. A. Cooperative symmetry-breaking by actin polymerisation in a model for cell motility. *Nature Cell Biol.* **1,** 493–499 (1999).
29. Beningo, K. A., Dembo, M., Kaverina, I., Small, J. V. & Wang, Y. Nascentfocal adhesions are responsible for the generation of strong propulsive forces in migrating fibroblasts. *J. Cell Biol.* **153,** 89–100 (2001).

Supplementary Information accompanies the paper on *Nature*'s website (http://www.nature.com).

Acknowledgements

We thank J. Plastino for discussions and the purification of VCA proteins, and F. Castellano and P. Chavrier for the gift of the plasmid encoding VCA. Theoretical discussions were conducted by J. Prost. We thank D. Didry for the purification of Arp2/3, ADF-cofilin, and actin, and R. Boujemaa for the purification of the capping protein. We thank H. Boukellal for help in determining the VCA concentration on the beads, E. Paluch for helping in analysing the videos and K. Sekimoto and D. Pantaloni for discussions.

Correspondence and request for material should be addressed to C.S. (e-mail: cecile.sykes@curie.fr), or M.-F.C. (e-mail: carlier@lebs.caps-gif.fr) for the motility medium.

Rotavirus protein involved in genome replication and packaging exhibits a HIT-like fold

Hariharan Jayaram*, Zenobia Taraporewala†, John T. Patton† & B. V. Venkataram Prasad*

** Program in Structural and Computational Biology and Molecular Biophysics, Verna and Marrs McLean Department of Biochemistry and Molecular Biology, Baylor College of Medicine, Houston, Texas 77030, USA*
† Laboratory of Infectious Diseases, National Institutes of Allergy and Infectious Diseases, National Institutes of Health, Bethesda, Maryland 20892, USA

Rotavirus, the major cause of life-threatening infantile gastroenteritis, is a member of the *Reoviridae*[1]. Although the structures of rotavirus[2] and other members of the *Reoviridae*[3,4] have been extensively studied, little is known about the structures of virus-encoded non-structural proteins that are essential for genome replication and packaging. The non-structural protein NSP2 of rotavirus, which exhibits nucleoside triphosphatase, single-stranded RNA binding[5], and nucleic-acid helix-destabilizing[6] activities, is a major component of viral replicase complexes[7,8]. We present here the X-ray structure of the functional octamer[9] of NSP2 determined to a resolution of 2.6 Å. The NSP2 monomer has two distinct domains. The amino-terminal domain has a new fold. The carboxy-terminal domain resembles the ubiquitous cellular histidine triad (HIT) group of nucleotidyl hydrolases[10]. This structural similarity suggests that the nucleotide-binding site is located inside the cleft between the two domains. Prominent grooves that run diagonally across the doughnut-shaped octamer are probable locations for RNA binding. Several RNA binding sites, resulting from the quaternary organization of NSP2 monomers, may be required for the helix destabilizing activity of NSP2 and its function during genome replication and packaging.

Rotavirus is a large and complex virus. Its genome, enclosed within three concentric capsid layers, consists of 11 segments of double-stranded RNA (dsRNA) that code for six structural and six non-structural proteins (NSPs)[1]. Several *in vivo* and *in vitro* studies have strongly implicated NSP2, a highly basic protein of relative molecular mass $M_r = 35{,}000$ which exits as octamers, in genome replication and packaging. This protein, in association with viral RNA and polymerase, localizes to viroplasms of the infected cells where these processes occur[7,11,12]. Temperature-sensitive mutants of NSP2 fail to replicate the genome and produce mostly empty particles, which implicates NSP2 in genome replication and packaging[13,14]. Recent studies on recombinant NSP2 have shown that it is a magnesium-dependent NTPase that binds to ssRNA in a sequence-independent manner[5] and exhibits nucleic-acid helix-destabilizing activity[6]. On the basis of these studies it is suggested that NSP2 functions as a molecular motor that uses the energy derived from NTP hydrolysis to package the viral genome[9]. In its function, NSP2 may be homologous to NS2 (refs 15, 16) of blue-tongue virus and σNS of orthoreovirus[17]. To understand the structural mechanisms underlying the function of NSP2, we have